Journal of Computational Physics 229 (2010) 5843–5856

Contents lists available at ScienceDirect

Journal of Computational Physics

journal homepage: www.elsevier.com/locate/jcp

Kinetic theory based lattice Boltzmann equation with viscous dissipation and pressure work for axisymmetric thermal flows

Lin Zheng, Zhaoli Guo *, Baochang Shi, Chuguang Zheng

National Laboratory of Coal Combustion, Huazhong University of Science and Technology, Wuhan 430074, China

ARTICLE INFO

Article history:
Received 18 October 2009
Received in revised form 7 February 2010
Accepted 14 April 2010
Available online 18 April 2010

Keywords:
Lattice Boltzmann equation
Axisymmetric thermal flow
Kinetic theory
Buoyancy-driven flow

ABSTRACT

A lattice Boltzmann equation (LBE) for axisymmetric thermal flows is proposed. The model is derived from the kinetic theory which exhibits several features that distinguish it from other previous LBE models. First, the present thermal LBE model is derived from the continuous Boltzmann equation, which has a solid foundation and clear physical significance; Second, the model can recover the energy equation with the viscous dissipation term and work of pressure which are usually ignored by traditional methods and the existing thermal LBE models; Finally, unlike the existing thermal LBE models, no velocity and temperature gradients appear in the force terms which are easy to realize in the present model. The model is validated by thermal flow in a pipe, thermal buoyancy-driven flow, and swirling flow in vertical cylinder by rotating the top and bottom walls. It is found that the numerical results agreed excellently with analytical solution or other numerical results.

1. Introduction

The axisymmetric thermal flows in the axisymmetric system is of great interest in fluid mechanics [1–3]. In the last two decades, LBE has been rapidly developed as an effective and promising numerical algorithm for computational fluid dynamics [4–6], which has also been applied to axisymmetric flows [7–19]. The straightforward way for LBE to simulate such flows is using a 3D LBE model with suitable curved boundary treatments [22–24]. Nevertheless, such approach implies the expensive computational costs for this 3D simulation which does not consider any symmetrical properties of the axisymmetric flows. Considered the properties of the axisymmetric flows, such flows can be reduced to a quasi-two-dimensional problems in the meridian plane. Although the LBE method has achieved great success in simulating axisymmetric athermal/isothermal fluid flows, it still has many challenges for constructing an effective and applicable axisymmetric LBE model.

In the literature, there are three categories of axisymmetric LBE models proposed for axisymmetric athermal flows [10–16], i.e., the coordinate transformation method (CTM), the vorticity–stream method (VSM) and the double-distribution-function (DDF) method. The main idea of CTM is that it transforms the axisymmetric Navier–Stokes equations (NSE) to the specific pseudo-Cartesian forms with some additional terms in these quasi-two-dimensional NSE. The CTM was introduced by Halliday et al. [10], who first proposed an axisymmetric D2Q9 model by adding some source terms into LBE so that it could recover the axisymmetric NSE at the macroscopic level. However, Lee et al. [11] found that some terms are missing in this model which would lead to large errors for simulating the constricted or expanded pipe flows. Later, Reis and Phillips [12,13] and Zhou [14] developed similar models based on the axisymmetric NSE. On the other hand, the VSM is another version of transformation method, it uses the relations between the vorticity, the stream function and the velocity, then the 3D axisymmetric NSE can be transformed to the vorticity–stream-function equations. Based on the vorticity–stream-function

* Corresponding author.
E-mail address: zlguo@hust.edu.cn (Z. Guo).

0021-9991/$ - see front matter © 2010 Elsevier Inc. All rights reserved.
doi:10.1016/j.jcp.2010.04.026

equations, Chen et al. [15] constructed a LBE model, but the model must solve a Poisson equation at each time step. It should be mentioned that the effect of azimuthal velocity is neglected by most of the above mentioned LBE models. Recently, considered the effect of the azimuthal velocity, the DDF method is first proposed by Guo et al. [16] for simulating athermal axisymmetric flow from the Boltzmann equation, one is for solving the axial and radial velocity components, and the other is for solving azimuthal velocity. This DDF method has a solid theory foundation and clear physical significance, and the main difference between Guo et al.'s model and the other existing models is that Guo et al.'s model is designed in a bottom-up fashion but the other existing models are designed in a top-down fashion.

However, the aforementioned LBE models are restricted to athermal axisymmetric flows, while very few axisymmetric LBE models proposed for axisymmetric thermal problems. To the authors' knowledge, only four works [17–20] applied the LBE to the axisymmetric thermal flows. These models can be classified into two categories, i.e., the hybrid approach and the double-distribution-function (DDF) method. The hybrid method is directly applied athermal axisymmetric LBE model to simulate the flow field, while the energy equation is solved by different numerical methods rather than solving LBE [17,18]. The DDF method utilizes two different density distribution functions similar to the athermal DDF approach, one is for solving the vorticity–stream-function equations or the NSE, and the other is for solving the energy equation [19,20]. The main difference between the DDF method and the hybrid method is that the energy equation is solved by LBE.

The application of hybrid approach and DDF method for axisymmetric thermal flows encountered many challenges. The fundamental problem with most of the hybrid LBE models [17,18] is that they directly used the athermal axisymmetric CTM LBE models to solve the flow field, which have the complicated force terms. Furthermore, due to the complicated force terms, the numerical instability is another critical problem for these hybrid methods, although the stability is improved by the modified model [18]. On the other hand, although the DDF approach proposed by Chen et al. [19] has greatly improved the numerical stability, and the complex force terms have been simplified, the model has to solve the Poisson equation at each time step as the limitation of their athermal model. Moreover, in Ref. [20], Zheng et al. pointed out this model seems to mismatch the energy equation at the macroscopic level, and proposed another version of DDF LBE model which can overcome this problem, and the force terms in the model have no velocity and temperature gradients. However, it should be pointed out that the existing axisymmetric thermal LBE models usually ignore the effect of viscous dissipation term and work of pressure in the energy equation. Therefore, it is desirable to construct a more general axisymmetric LBE model for axisymmetric thermal flows.

In sight of the limitations in the previous works, in this paper, we aim to propose an axisymmetric thermal LBE model from the continuous Boltzmann equation, which could recover the energy equation with the viscous dissipation term and work of pressure. The rest of the paper is organized as follows. In Section 2, kinetic theory of axisymmetric Boltzmann equation is introduced. In Section 3, the axisymmetric thermal LBE model derived from the continuous Boltzmann equation, and some numerical tests of the LBE model are conducted in Section 4, and finally a brief conclusion is presented in Section 5.

2. Kinetic theory of axisymmetric Boltzmann equation

The fully axisymmetric Boltzmann equation including an external force with the Bhatnagar–Gross–Krook (BGK) collision operator for symmetric flows is given as

$$\frac{\partial f}{\partial t}+\xi_x\frac{\partial f}{\partial x}+\xi_r\frac{\partial f}{\partial r}+\frac{\xi_\theta^2}{r}\frac{\partial f}{\partial \xi_r}-\frac{\xi_r\xi_\theta}{r}\frac{\partial f}{\partial \xi_\theta}+\boldsymbol{a}_0\cdot\frac{\partial f}{\partial_{\xi_0}}=-\frac{1}{\tau_f}[f-f^{(eq)}], \tag{1}$$

where $f(\boldsymbol{x},\boldsymbol{\xi}_0,t)\equiv f(x,r,\xi_x,\xi_r,\xi_\theta,t)$ is the density distribution function of fluid molecules moving with velocity $\boldsymbol{\xi}_0=(\xi_x,\xi_r,\xi_\theta)$ at position $\boldsymbol{x}=(x,r)$ and time t in the cylindrical coordinates, $\boldsymbol{a}_0=(a_x,a_r,a_\theta)$ is the external force, τ_f is relaxation time and $f^{(eq)}$ is local Maxwellian equilibrium distribution defined by

$$f^{(eq)}=\frac{\rho}{(2\pi RT)^{3/2}}\exp\left[-\frac{|\boldsymbol{\xi}_0-\boldsymbol{u}_0|^2}{2RT}\right], \tag{2}$$

where R is gas constant, ρ, $\boldsymbol{u}_0=(u_x,u_r,u_\theta)$ with u_x, u_r and u_θ being axial, radial and azimuthal velocity components, and T are respectively the fluid density, velocity and temperature defined by,

$$\rho=\int f\,d\boldsymbol{\xi}_0,\quad \rho\boldsymbol{u}_0=\int \boldsymbol{\xi}_0 f\,d\boldsymbol{\xi}_0,\quad 3\rho RT=\int|\boldsymbol{\xi}_0-\boldsymbol{u}_0|^2 f\,d\boldsymbol{\xi}_0, \tag{3}$$

As the similar procedure as Ref. [16], we introduce the following reduced distribution functions

$$\tilde{f}(\boldsymbol{x},\boldsymbol{\xi})=\int f\,d\xi_\theta,\quad \bar{f}(\boldsymbol{x},\boldsymbol{\xi})=\int \xi_\theta f\,d\xi_\theta,\quad \hat{f}(\boldsymbol{x},\boldsymbol{\xi})=\int\frac{|\boldsymbol{\xi}_0|^2}{2}f\,d\xi_\theta, \tag{4}$$

and then Eq. (1) can be simplified to the following three equations

$$\frac{\partial \tilde{f}}{\partial t}+\boldsymbol{\xi}\cdot\nabla\tilde{f}+\boldsymbol{a}\cdot\nabla_{\xi}\tilde{f}+\frac{\xi_r}{r}\tilde{f}+\frac{1}{r}\frac{\partial\tilde{\phi}}{\partial\xi_r}=-\frac{1}{\tau_f}[\tilde{f}-\tilde{f}^{(eq)}], \tag{5}$$

$$\frac{\partial \bar{f}}{\partial t}+\boldsymbol{\xi}\cdot\nabla\bar{f}+\boldsymbol{a}\cdot\nabla_{\xi}\bar{f}+\frac{2\xi_r}{r}\bar{f}+\frac{1}{r}\frac{\partial\bar{\phi}}{\partial\xi_r}=-\frac{1}{\tau_f}[\bar{f}-\tilde{f}^{(eq)}], \tag{6}$$

$$\frac{\partial \hat{f}}{\partial t}+\boldsymbol{\xi}\cdot\nabla\hat{f}+\boldsymbol{a}\cdot\nabla_{\xi}\hat{f}-\boldsymbol{a}\cdot\boldsymbol{\xi}\tilde{f}-a_\theta\bar{f}+\frac{\xi_r}{r}\hat{f}+\frac{1}{2r}\frac{\partial\hat{\Phi}}{\partial\xi_r}=-\frac{1}{\tau_f}[\hat{f}-\hat{f}^{(eq)}], \tag{7}$$

where $\boldsymbol{\xi}=(\xi_x,\xi_r)$, $\nabla=(\partial_x,\partial_r)$, $\nabla_\xi=(\partial_{\xi_x},\partial_{\xi_r})$, $\boldsymbol{a}=(a_x,a_r)$ the external force in the meridian plane, and

$$\tilde{\phi}(\boldsymbol{x},\boldsymbol{\xi})=\int\xi_\theta^2 f\,d\xi_\theta,\quad \bar{\phi}(\boldsymbol{x},\boldsymbol{\xi})=\int\xi_\theta^3 f\,d\xi_\theta,\quad \hat{\Phi}(\boldsymbol{x},\boldsymbol{\xi})=\xi^2\tilde{\phi}+\int\xi_\theta^4 f\,d\xi_\theta. \tag{8}$$

From Eq. (4), the corresponding equilibrium distribution functions can be derived as following:

$$\tilde{f}^{(eq)}=\frac{\rho}{(2\pi RT)}\exp\left[-\frac{|\boldsymbol{\xi}-\boldsymbol{u}|^2}{2RT}\right],\quad \bar{f}^{(eq)}=u_\theta\tilde{f}^{(eq)},\quad \hat{f}^{(eq)}=\frac{\xi^2+u_\theta^2+RT}{2}\tilde{f}^{(eq)}, \tag{9}$$

where $\boldsymbol{u}=(u_x,u_r)$ is the velocity in x–r plane. The fluid density, velocity and the total energy can be defined as

$$\rho=\int\tilde{f}\,d\boldsymbol{\xi}_0,\quad \rho\boldsymbol{u}=\int\boldsymbol{\xi}\bar{f}\,d\boldsymbol{\xi},\quad \rho u_\theta=\int\bar{f}\,d\boldsymbol{\xi},\quad \rho E=\int\hat{f}\,d\boldsymbol{\xi}, \tag{10}$$

where $E=c_vT+\boldsymbol{u}_0/2$, and c_v is the specific heat coefficient at constant volume.

Through Chapman–Enskog expansion technique [25], the macroscopic axisymmetric equations can be recovered as (see Appendix A for details)

$$\partial_t\rho+\partial_\alpha(\rho u_\alpha)+\frac{\rho u_r}{r}=0, \tag{11}$$

$$\begin{aligned}\partial_t(\rho u_\alpha)+\partial_\beta(\rho u_\alpha u_\beta+p\delta_{\alpha\beta})=&\partial_\beta\left[\mu\left(\partial_\alpha u_\beta+\partial_\beta u_\alpha-\left(\partial_\gamma u_\gamma+\frac{u_r}{r}\right)\delta_{\alpha\beta}\right)\right]+\frac{\mu}{r}\left[\partial_\alpha u_r+\partial_r u_\alpha-\left(\partial_\gamma u_\gamma+\frac{u_r}{r}\right)\delta_{\alpha r}\right]\\&+\frac{\rho u_\theta^2}{r}\delta_{\alpha r}-\frac{\rho u_\alpha u_r}{r}-\frac{2\mu}{r^2}u_r\delta_{\alpha r}+\rho a_\alpha,\end{aligned} \tag{12}$$

$$\partial_t(\rho u_\theta)+\partial_\beta(\rho u_\beta u_\theta)=\partial_\beta(\mu\partial_\beta u_\theta)-\frac{2\rho u_\theta u_r}{r}-\frac{\mu}{r}\left(u_\theta\partial_r\ln\rho-\partial_r u_\theta+\frac{u_\theta}{r}\right)+\rho a_\theta, \tag{13}$$

$$\begin{aligned}\partial_t\rho E+\partial_\alpha[(\rho E+p)u_\alpha]+\frac{1}{r}[(\rho E+p)u_r]=&\partial_\alpha(\lambda\partial_\alpha T)+\partial_\alpha\left[\mu u_\beta\left(\partial_\alpha u_\beta+\partial_\beta u_\alpha-\left(\partial_\gamma u_\gamma+\frac{u_r}{r}\right)\delta_{\alpha\beta}\right)\right]+\partial_\alpha(\mu u_\theta\partial_\alpha u_\theta)\\&-\partial_r\left(\frac{\mu u_\theta^2}{r}\right)+\frac{1}{r}\left[\lambda\partial_r T+\mu\left(u_\beta\left(\partial_r u_\beta+\partial_\beta u_r-\left(\partial_\gamma u_\gamma+\frac{u_r}{r}\right)\delta_{r\beta}\right)\right)\right.\\&\left.+\mu u_\theta\partial_r u_\theta-\frac{\mu u_\theta^2}{r}\right]+\rho u_{0\alpha}a_\alpha,\end{aligned} \tag{14}$$

where $\mu=\tau_f p$ is the dynamic viscosity and $\lambda=c_p\tau_f p$ is the thermal conductivity with c_p being the specific heat coefficient at constant pressure.

In this LBE model, both the dynamic viscosity and thermal conductivity are related to the same relaxation time in Eq. (14). Therefore, the ratio of the dynamic viscosity and thermal conductivity is a constant in the energy equation, which cause to a fixed Prandlt number, $\mathrm{Pr}=c_p\mu/\lambda$. To remove this inconvenience, we multiplied $\xi_0^2/2$ on both side of Eq. (1) and rearranged the corresponding collision operator (Ω_h) motivated by the idea of Guo et al. [21], which can be written as

$$\Omega_h=-\frac{\xi_0^2}{2\tau_h}(f-f^{(eq)})+\frac{Z_0}{\tau_{hf}}[(f_i-f_i^{(eq)})],$$

where $1/\tau_{hf}=1/\tau_h-1/\tau_f$ with τ_h being the relaxation time, $Z_0=\boldsymbol{\xi}_0\cdot\boldsymbol{u}_0-\boldsymbol{u}_0^2/2$. Then we could get the following evolution equation from the axisymmetric Boltzmann equation (1) as

$$\frac{\partial \hat{f}}{\partial t}+\xi\cdot\nabla\hat{f}+\boldsymbol{a}\cdot\nabla_\xi\hat{f}-\boldsymbol{a}\cdot\boldsymbol{\xi}\tilde{f}-a_\theta\bar{f}+\frac{\xi_r}{r}\hat{f}+\frac{1}{2r}\frac{\partial\hat{\Phi}}{\partial\xi_r}=-\frac{1}{\tau_h}[\hat{f}-\hat{f}^{(eq)}]+\frac{1}{\tau_{hf}}[Z(\tilde{f}_i-\tilde{f}_i^{(eq)})+u_\theta(\bar{f}_i-\bar{f}_i^{(eq)})], \tag{15}$$

where $Z=\boldsymbol{\xi}\cdot\boldsymbol{u}-\boldsymbol{u}_0^2/2$.

With this modified collision operator, the dynamic viscosity and the thermal conductivity become to $\mu=\tau_f p$ and $\lambda=c_p\tau_h p$ respectively, and the fixed Prandtl number problem is removed in the energy equation.

3. Lattice Boltzmann model for axisymmetric thermal flow

In this section, we will derive the lattice Boltzmann equation from Eqs. (5), (6) and (15). With the assumption of $\boldsymbol{a}_0 \cdot \nabla_{\xi_0} f \approx \boldsymbol{a}_0 \cdot \nabla_{\xi_0} f^{(eq)}$, these three reduced equations can be rewritten as

$$\frac{\partial \tilde{f}}{\partial t} + \boldsymbol{\xi} \cdot \nabla \tilde{f} + \frac{\xi_r}{r}\tilde{f} = -\frac{1}{\tau_f}[\tilde{f} - \tilde{f}^{(eq)}] + \widetilde{F}', \tag{16}$$

$$\frac{\partial \bar{f}}{\partial t} + \boldsymbol{\xi} \cdot \nabla \bar{f} + \frac{2\xi_r}{r}\bar{f} = -\frac{1}{\tau_f}[\bar{f} - \bar{f}^{(eq)}] + \overline{F}', \tag{17}$$

$$\frac{\partial \hat{f}}{\partial t} + \boldsymbol{\xi} \cdot \nabla \hat{f} + \frac{\xi_r}{r}\hat{f} = -\frac{1}{\tau_h}[\hat{f} - \hat{f}^{(eq)}] + \widehat{F}', \tag{18}$$

where $\widetilde{F}'$ and $\overline{F}'$ are given as [16]

$$\widetilde{F}' = \frac{(\boldsymbol{\xi} - \boldsymbol{u}) \cdot \tilde{\boldsymbol{a}}}{RT}\tilde{f}^{(eq)}, \quad \overline{F}' = \frac{(\boldsymbol{\xi} - \boldsymbol{u}) \cdot \bar{\boldsymbol{a}}}{RT}\bar{f}^{(eq)} + a_\theta \tilde{f}^{(eq)},$$

and the term of $\widehat{F}'$ can be approximated by

$$\widehat{F}' = \frac{1}{\tau_{hf}}[Z(\tilde{f} - \tilde{f}^{(eq)}) + u_\theta(\bar{f} - \bar{f}^{(eq)})] + \omega(\boldsymbol{\xi}, T)\rho E\left[\frac{\boldsymbol{\xi} \cdot \boldsymbol{a}}{RT}\right] + \tilde{f}\boldsymbol{\xi} \cdot \boldsymbol{a} + a_\theta \bar{f} - \frac{1}{2r}\partial_{\xi_r}\widehat{\Phi}$$

with

$$\begin{aligned}\partial_{\xi_r}\widehat{\Phi} &\approx \partial_{\xi_r}\widehat{\Phi}^{(0)} \\ &= \left[2\xi_r + \left(\frac{u_\theta^2}{RT} + 1\right)(\xi_r - u_r)\right](u_\theta^2 + RT)\tilde{f}^{(eq)} - 2\left(\frac{u_\theta^2}{RT} + 1\right)(\xi_r - u_r)\hat{f}^{(eq)} - 3RT(\xi_r - u_r)\tilde{f}^{(eq)} - u_\theta\left(\frac{u_\theta^2}{RT} + 6\right)(\xi_r - u_r)\bar{f}^{(eq)}\end{aligned} \tag{19}$$

and

$$\tilde{a}_x = a_x, \quad \tilde{a}_r = a_r + \frac{RT}{r}\left(1 + \frac{u_\theta^2}{RT} - \frac{2\tau_f u_r}{r}\right), \tag{20}$$

$$\bar{a}_x = a_x, \quad \bar{a}_r = a_r + \frac{RT}{r}\left(3 + \frac{u_\theta^2}{RT}\right). \tag{21}$$

As indicated in Ref. [16], we cannot directly construct an efficient thermal LBE model from the above equations. The simplified forms of Eqs. (16) and (17) are obtained by Ref. [16] as follows

$$\frac{\partial f}{\partial t} + \boldsymbol{\xi} \cdot \nabla f = -\frac{1}{\tau_f}[f - f^{(eq)}] + F, \tag{22}$$

$$\frac{\partial g}{\partial t} + \boldsymbol{\xi} \cdot \nabla g = -\frac{1}{\tau_f}[g - g^{(eq)}] + G, \tag{23}$$

while for Eq. (18), we could transform it by multiplying r on both sides, and the compact form is given as

$$\frac{\partial h}{\partial t} + \boldsymbol{\xi} \cdot \nabla h = -\frac{1}{\tau_h}[h - h^{(eq)}] + H, \tag{24}$$

where $f = r\tilde{f}$, $f^{(eq)} = r\tilde{f}^{(eq)}$, $F = r\widetilde{F}'$, $g = r^2\bar{f}$, $g^{(eq)} = r^2\bar{f}^{(eq)}$, $G = r^2\overline{F}'$, $h = r\hat{f}$, $h^{(eq)} = r\hat{f}^{(eq)}$, $H = r\widehat{F}'$, and the fluid density, velocity, total energy are redefined by

$$\rho = \frac{1}{r}\int f\,d\xi, \quad \rho\boldsymbol{u} = \frac{1}{r}\int \xi f\,d\xi, \quad \rho u_\theta = \frac{1}{r^2}\int g\,d\xi, \quad \rho E = \frac{1}{r}\int h\,d\xi. \tag{25}$$

Integrating Eqs. (22)–(24) along the characteristic line from time t to $t + \delta t$ and using trapezoidal discretization rule, we introduce the following new distribution functions

$$\tilde{f}_i = f_i - \frac{\delta t}{2}(\Omega_{fi} + F_i), \tag{26}$$

$$\tilde{g}_i = g_i - \frac{\delta t}{2}(\Omega_{gi} + G_i), \tag{27}$$

$$\tilde{h}_i = h_i - \frac{\delta t}{2}(\Omega_{hi} + H_i), \tag{28}$$

and then we could obtain the evolution equation for the velocity field as [16]:

$$\tilde{f}_i(\boldsymbol{x}+\boldsymbol{c}_i\delta t,t+\delta t)-\tilde{f}_i(\boldsymbol{x},t)=-\omega_f[\tilde{f}_i(\boldsymbol{x},t)-f_i^{(eq)}(\boldsymbol{x},t)]+\delta t\Big(1-\frac{\omega_f}{2}\Big)F_i(\boldsymbol{x},t), \tag{29}$$

$$\tilde{g}_i(\boldsymbol{x}+\boldsymbol{c}_i\delta t,t+\delta t)-\tilde{g}_i(\boldsymbol{x},t)=-\omega_f[\tilde{g}_i(\boldsymbol{x},t)-g_i^{(eq)}(\boldsymbol{x},t)]+\delta t\Big(1-\frac{\omega_f}{2}\Big)G_i(\boldsymbol{x},t) \tag{30}$$

with $i=0,1,\ldots,8$, where $\omega_f=2\delta t/(2\tau_f+\delta t)$, the equilibrium distribution functions $f_i^{(eq)}$, $g_i^{(eq)}$ and the forcing terms F_i and G_i are respectively given by [16]

$$f_i^{(eq)}=r\omega_i\rho\left\{1+\frac{\boldsymbol{c}_i\cdot\boldsymbol{u}}{RT}+\frac{1}{2}\left[\Big(\frac{\boldsymbol{c}_i\cdot\boldsymbol{u}}{RT}\Big)^2-\frac{u^2}{RT}\right]\right\},\quad g_i^{(eq)}=ru_\theta f_i^{(eq)}, \tag{31}$$

$$F_i=\frac{(\boldsymbol{c}_i-\boldsymbol{u})\cdot\tilde{\boldsymbol{a}}}{RT}f_i^{(eq)},\quad G_i=\frac{(\boldsymbol{c}_i-\boldsymbol{u})\cdot\tilde{\boldsymbol{a}}}{RT}g_i^{(eq)}+ra_\theta f_i^{(eq)}, \tag{32}$$

where $\omega_0=4/9$, $\omega_{1-4}=1/9$ and $\omega_{5-8}=1/36$ are the weight coefficients and

$$\boldsymbol{c}_i=(c_{ix},c_{ir})=\begin{cases}(0,0), & i=0,\\ (\cos[(i-1)\pi/2],\sin[(i-1)\pi/2])c, & i=1\text{–}4,\\ (\cos[(2i-9)\pi/4],\sin[(2i-9)\pi/4])\sqrt{2}c, & i=5\text{–}8,\end{cases} \tag{33}$$

where $c=\sqrt{3RT}=\delta x/\delta t$ with δx being the lattice space and δt the time step.

For the temperature field, the evolution equation can be derived from Eq. (24), which reads

$$\tilde{h}_i(\boldsymbol{x}+\boldsymbol{c}_i\delta t,t+\delta t)-\tilde{h}_i(\boldsymbol{x},t)=-\omega_h[\tilde{h}_i(\boldsymbol{x},t)-h_i^{(eq)}(\boldsymbol{x},t)]+\delta t\Big(1-\frac{\omega_h}{2}\Big)H_i(\boldsymbol{x},t), \tag{34}$$

where $\omega_h=2\delta t/(2\tau_h+\delta t)$, the equilibrium distribution function $h_i^{(eq)}$ is given as

$$h_h^{(eq)}=\omega_i rp\left[\frac{\boldsymbol{c}_i\cdot\boldsymbol{u}}{RT}+\Big(\frac{\boldsymbol{c}_i\cdot\boldsymbol{u}}{RT}\Big)^2+\frac{c_i^2}{2RT}-\frac{u^2}{RT}-1\right]+Ef_i^{(eq)}, \tag{35}$$

and the source term, H_i, can be decomposed into two parts, i.e., $H_i=H_{1i}+H_{2i}$, where

$$H_{1i}=\frac{1}{\tau_{hf}}\left[Z_i(f_i-f_i^{(eq)})+\frac{u_\theta}{r}(g_i-g_i^{(eq)})\right] \tag{36}$$

$$\begin{aligned}H_{2i}=&\omega_i r\rho E\Big[\frac{\boldsymbol{c}_i\cdot\boldsymbol{a}}{RT}\Big]+f_i\boldsymbol{c}_i\cdot\boldsymbol{a}+\frac{a_\theta}{r}g_i\\&-\frac{1}{2}\left\{\left[(2c_{ir}RT+(u_\theta^2+RT)(c_{ir}-u_r))f_i^{(eq)}-(c_{ir}-u_r)\frac{2}{rRT}h_i^{(eq)}\right](u_\theta^2+RT)-(c_{ir}-u_r)\left[3RTf_i^{(eq)}+\frac{u_\theta}{r}\Big(\frac{u_\theta^2}{RT}+6\Big)g_i^{(eq)}\right]\right\}\end{aligned} \tag{37}$$

with $Z_i=\boldsymbol{c}_i\cdot\boldsymbol{u}-\boldsymbol{u}_0^2/2$. Noting that $(1+\delta t/2\tau_f)^{-1}/\tau_{hf}=(\omega_h-\omega_f)/\delta t(1-\omega_h/2)$, we can rewrite Eq. (34) as

$$\begin{aligned}\tilde{h}_i(\boldsymbol{x}+\boldsymbol{c}_i\delta t,t+\delta t)-\tilde{h}_i(\boldsymbol{x},t)=&-\omega_h[\tilde{h}_i(\boldsymbol{x},t)-h_i^{(eq)}(\boldsymbol{x},t)]+(\omega_h-\omega_f)\left[Z_i(f_i-f_i^{(eq)})+\frac{u_\theta}{r}(g_i-g_i^{(eq)})\right]\\&+\delta t\Big(1-\frac{\omega_h}{2}\Big)H_{2i}(\boldsymbol{x},t),\end{aligned} \tag{38}$$

The fluid density, velocity and total energy defined by the velocity moments of the new distribution functions are given by

$$\rho=\frac{1}{r}\sum_i\tilde{f}_i, \tag{39}$$

$$\rho u_\theta=\frac{1}{r^2}\sum_i\tilde{g}_i+\frac{\delta t}{2}\rho a_\theta, \tag{40}$$

$$\rho u_\alpha=\frac{r}{r^2+\tau_f\delta tRT\delta_{\alpha r}}\left\{\sum_i c_{i\alpha}\tilde{f}_i+\frac{\delta t}{2}\rho\left[ra_\alpha+(u_\theta^2+RT)\delta_{\alpha r}\right]\right\}, \tag{41}$$

$$\rho E=\frac{1}{r}\sum_i\tilde{h}_i+\frac{\delta t}{2}\rho\boldsymbol{u}_0\cdot\boldsymbol{a}_0, \tag{42}$$

Now some remarks on the present thermal model are given as follows: First, the present thermal model is derived from the axisymmetric Boltzmann equation, which has a solid foundation. Second, owing to the clearly kinetic background, the viscous dissipation term and work of pressure are included by present model, which are usually neglected by the traditional methods and the existing axisymmetric thermal LBE models. Third, the source term, H_i, given by Eqs. (36) and (37), has no

velocity and temperature gradients which inherit the simple algorithm of LBE. Finally, in some special cases, the azimuthal velocity u_θ is usually absent, therefore, the evolution equation for the azimuthal velocity can be neglected, and the external force term, F_i, given by Eq. (32), can be simplified as

$$F_i = \frac{(\boldsymbol{c}_i - \boldsymbol{u}) \cdot \tilde{\boldsymbol{a}}}{RT} f_i^{(eq)},$$

and the simplification of H_{1i} and H_{2i} in source term, H_i, can be given as,

$$H_{1i} = \frac{1}{\tau_{hf}}[Z_i(f_i - f_i^{(eq)})],$$
$$H_{2i} = \omega_i r \rho E\left[\frac{\boldsymbol{c}_i \cdot \boldsymbol{a}}{RT}\right] + f_i \boldsymbol{c}_i \cdot \boldsymbol{a} - u_r RT f_i^{(eq)} + \frac{c_{ir} - u_r}{r} h_i^{(eq)},$$

where

$$\tilde{a}_x = a_x, \quad \tilde{a}_r = a_r + \frac{RT}{r}\left(1 - \frac{2\tau_f u_r}{r}\right), \tag{43}$$

and if no external force acts on the flow, H_{2i} can be further simplified as

$$H_{2i} = -u_r RT f_i^{(eq)} + \frac{c_{ir} - u_r}{r} h_i^{(eq)}.$$

4. Numerical tests

In this section, we will conduct some numerical tests to validate the proposed thermal model. The test problems include the thermal flow in a pipe, and two different kinds of nontrivial thermal buoyancy-driven flows in a cylindrical enclosure, that is, natural convection in a laterally heated and upper cooled vertical cylinder, and heat transfer of swirling flows in cylindrical container with co-/counter-rotating walls. In our simulations, the symmetry boundary condition (SBC) [16] and non-equilibrium extrapolation boundary treatment (NEEBT) [26] are applied to the symmetry axis and other boundaries respectively for all cases.

4.1. Thermal flow in a pipe

The first test problem is the thermal Hagen–Poiseuille flow through a straight pipe of radius R driven by a constant external force $\boldsymbol{a} = (a_x, 0)$. The computational domain is $0 \leqslant x \leqslant L$ and $0 \leqslant r \leqslant R$, where $r = 0$ is the symmetric axis and the solid wall is located at $r = R$ with constant temperature $T_w = 1.0$. The boundary conditions for the fluid variables are as follows:

$$r = 0: \ \frac{\partial \phi}{\partial r} = 0, \quad \forall \phi;$$
$$r = R: \ u_x = u_r = 0, \quad T = T_w.$$

Periodic boundary condition is applied to the x direction, the steady axial velocity and temperature profiles for this problem can be described as

$$u_x(r) = u_0\left(1 - \frac{r^2}{R^2}\right), \tag{44}$$

$$T(r) = T_w + \frac{\Pr u_0^2}{4c_v}\left[1 - \frac{r^4}{R^4}\right], \tag{45}$$

where $u_0 = a_z R^2/4\nu$ is the maximum velocity.

In the simulation, a $N_r \times N_x = 40 \times 60$ lattice is employed, and periodic boundary condition is applied to the x direction. Fig. 1(a) compares the temperature predicted by the present LBE with the analytical solutions for $\mathrm{Re} = 2Ru_0/\nu = 50$ as Pr varies from 0.2 to 4.0, while temperature profile for $\Pr = 0.7$ with Re varying from 20 to 100 are shown in Fig. 1(b). It is shown that the numerical results agree excellently with the analytical ones. The viscous dissipation effects are successfully captured by the present thermal LBE model over a wide range of the values of Pr and Re numbers.

4.2. Natural convection in a vertical cylinder

Natural convection flow in a square cavity has been studied extensively by experiment and traditional numerical methods, but it is quite rare for LBE [19,20]. Unless otherwise mentioned, in the present study, the computational domain with the aspect ratio $Al = H/D = 1/2$ is shown in Fig. 2, where H is the height of the vertical cylinder and D is the diameter. The boundary conditions are the same as Ref. [3,19,20], that is, the bottom wall is insulated, while the lateral wall is heated with a uniform flux $\partial T/\partial r = 1$, and a uniform flux, $\partial T/\partial x = -2$, is used for cooling the upper wall.

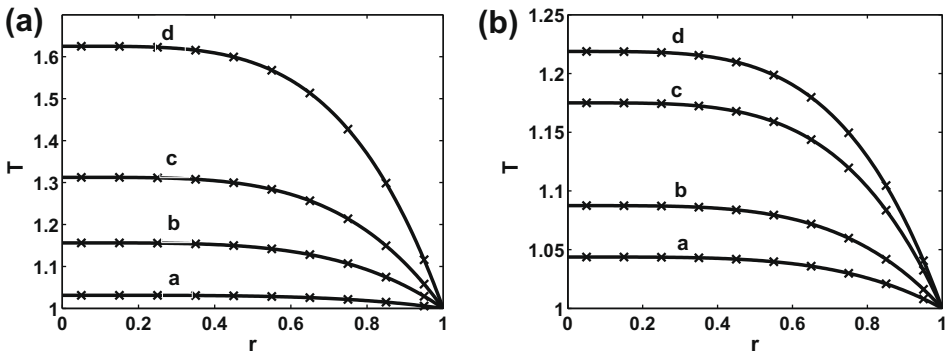

Fig. 1. Temperature profiles compared with the analytical solutions. (a) Re = 50, a–d: Pr = 0.2, 1.0, 2.0, 4.0; (b) Pr = 0.7, a–d: Re = 20, 40, 80, 100.

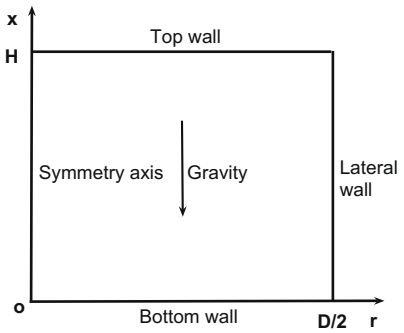

Fig. 2. Cross-section of the computational domain.

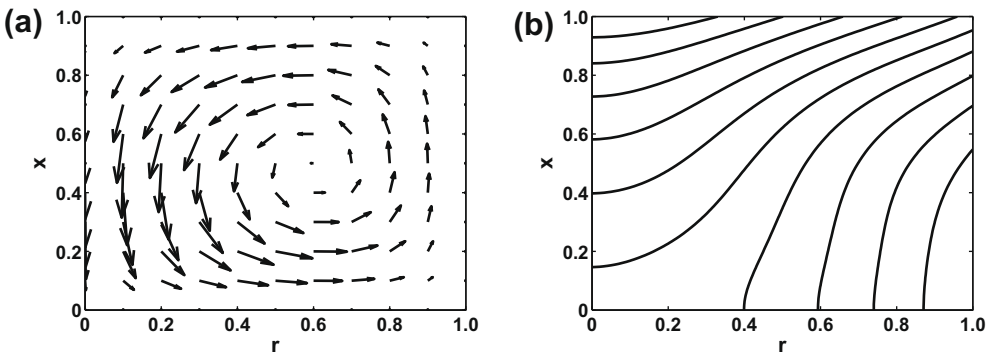

Fig. 3. Flow field (a) and isothermal lines (b) at $Ra = 10^3$.

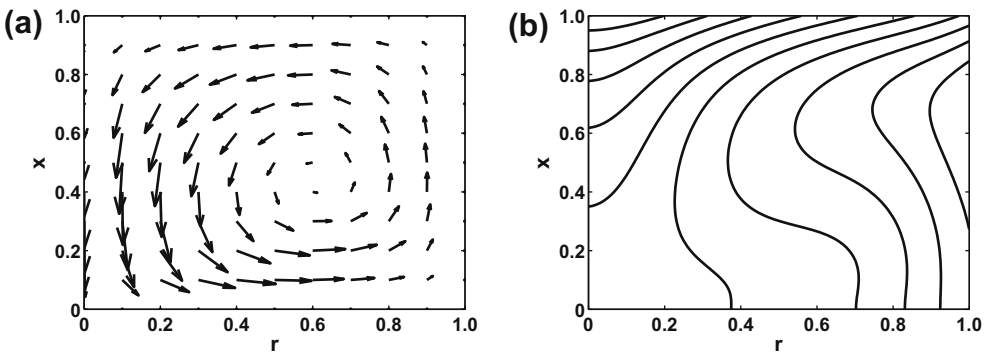

Fig. 4. Flow field (a) and isothermal lines (b) at $Ra = 10^4$.

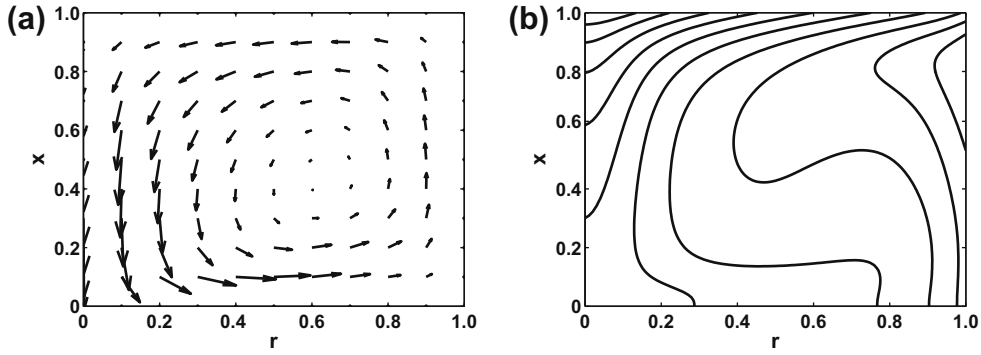

Fig. 5. Flow field (a) and isothermal lines (b) at Ra = 10^5.

Table 1
Comparisons of the LBE results with Refs. [3,19,20].

Ra		V_{max}	T_{min}	T_{max}	Nu_t	Nu_l
10^3	Ref. [3]	0.2391	−0.93	0.50	7.4604	6.6698
	Ref. [19]	0.2350	–	–	7.0663	6.2879
	Ref. [20]	0.2397	−0.9377	0.5051	7.4927	6.6215
	Ec $\sim O(10^{-30})$	0.2395	−0.9454	0.5005	7.5528	6.6348
	Ec $\sim O(1)$	0.6036	1.2314	3.5619	1.4302	3.3226
10^4	Ref. [3]	0.4143	−0.69	0.30	14.5255	9.0678
	Ref. [19]	0.4075	–	–	14.2291	8.9658
	Ref. [20]	0.4135	−0.6926	0.3075	14.7171	9.0836
	Ec $\sim O(10^{-30})$	0.4136	−0.7051	0.2977	14.8222	9.0837
	Ec $\sim O(1)$	0.5143	−0.0235	1.1250	5.4280	7.4380
10^5	Ref. [3]	0.4552	−0.52	0.21	24.3568	14.3750
	Ref. [19]	0.4547	–	–	23.9619	14.2782
	Ref. [20]	0.4593	−0.5348	0.2149	24.9140	14.3837
	Ec $\sim O(10^{-30})$	0.4594	−0.5355	0.2147	24.5256	14.3841
	Ec $\sim O(1)$	0.4852	−0.1861	0.6204	12.3136	12.5339

We first study this convection problem at the Eckert number $Ec = u_r^2/c_p\Delta T_0$ being set to be less than 10^{-30} with u_r and ΔT_0 being respectively the reference velocity and the reference temperature difference, which means that the viscous dissipation term and pressure work could be neglected, and the simulation is carried out on a 100×100 mesh at Pr = 0.7 as Ra varies from 10^3 to 10^5. The velocity and isothermal lines predicted by present model are shown in Figs. 3–5. It is found that for low Ra, the isotherms are slightly deformed and the highest temperature appears in the lower corner of the cylinder, and the isotherms become much more deformed as Ra increases. All of these observations are similar to that in previous studies [3,20]. To quantify the comparison, the maximum velocity, minimum and maximum temperature, and the average Nusselt numbers for lateral (Nu_l) and top (Nu_t) walls are also measured and compared with the works of Refs. [3,19,20] in Table 1. It is found that the numerical results predicted by the present model agreed well with previous studies [3,19,20].

The effect of the viscous dissipation term is also investigated by the present model with $Ec \sim O(1)$. The isothermal lines are shown in Fig. 6, and the maximum velocity, minimum and maximum temperature, and the average Nusselt numbers for

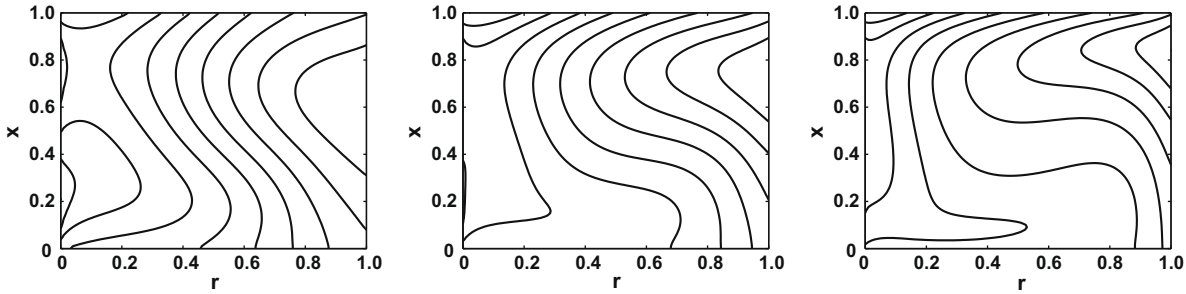

Fig. 6. Effect of viscous dissipation on isothermal lines: left to right Ra = 10^3, 10^4 and 10^5.

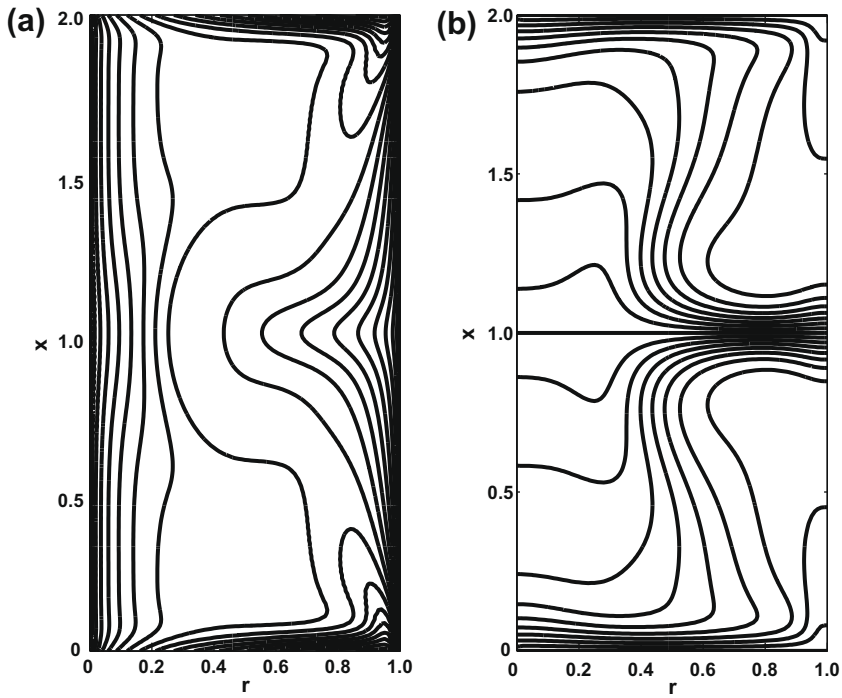

Fig. 7. Contour of azimuthal velocity component (a) and isothermal lines (b) at Re = 1000, Ri = 0, and $s = 1$.

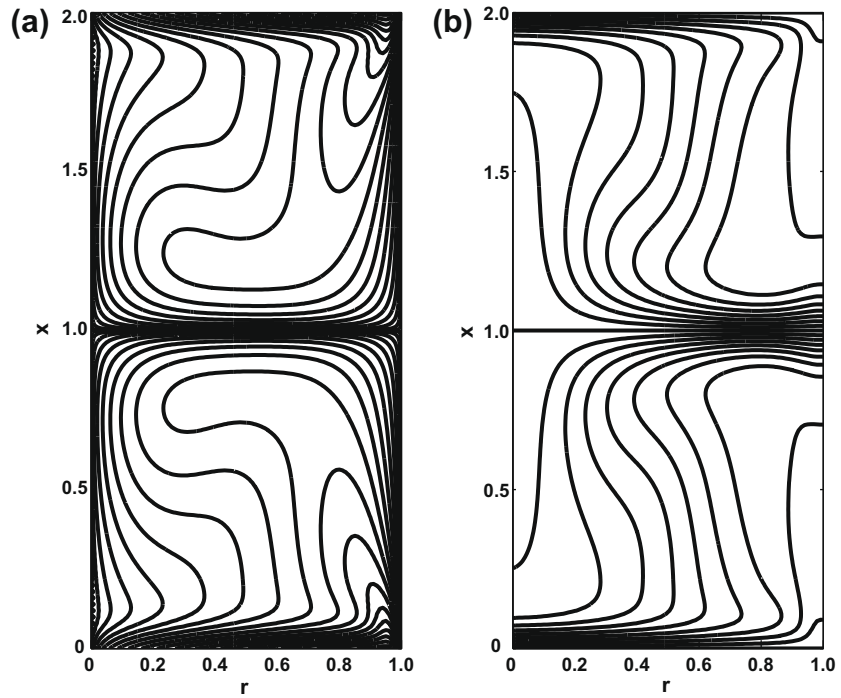

Fig. 8. Contour of azimuthal velocity component (a) and isothermal lines (b) at Re = 1000, Ri = 0, and $s = -1$.

lateral and top walls are included in the last line for each Ra number. It is seen that the isothermal lines in Fig. 6 are quite different from that in Figs. 3–5. In Table 1, it is found that as to the effect of the viscous dissipation term the maximum velocity and minimum temperature decrease as Ra increases, while they increase without the viscous dissipation term, implying that the viscous dissipation term cannot be ignored in some special cases.

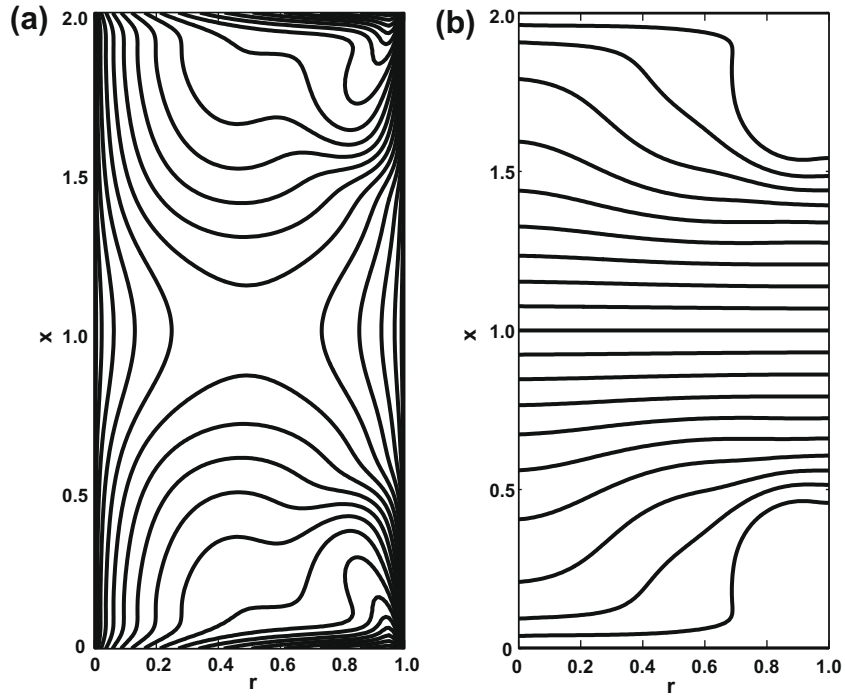

Fig. 9. Contour of azimuthal velocity component (a) and isothermal lines (b) at Re = 1000, Ri = 1, and $s = 1$.

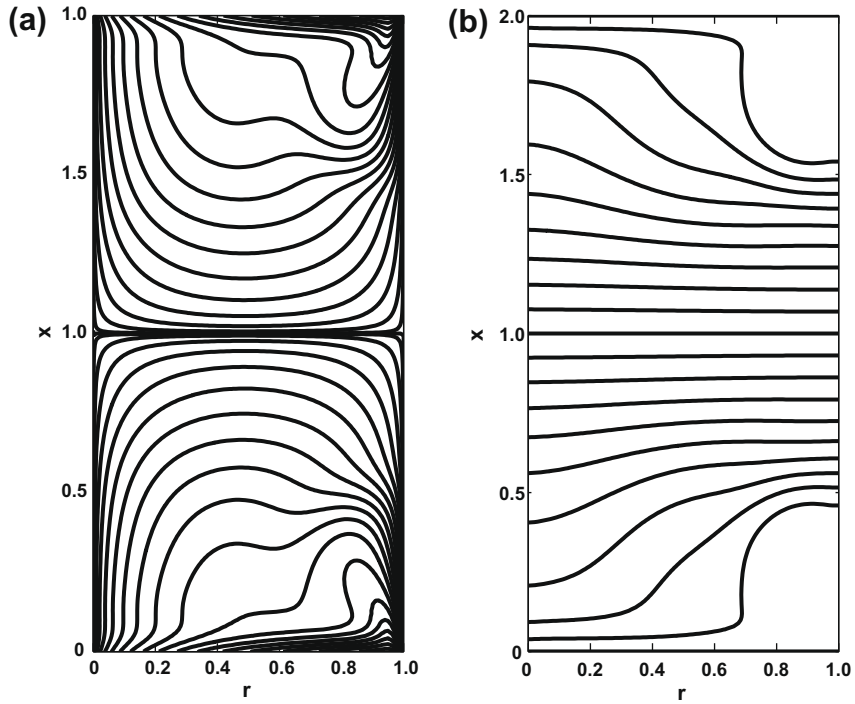

Fig. 10. Contour of azimuthal velocity component (a) and isothermal lines (b) at Re = 1000, Ri = 1, and $s = -1$.

4.3. Swirling flows in vertical cylinder with co-/counter-rotating walls

In this section, we will validate the proposed model by simulating swirling flows with a constant temperature gradient in a vertical cylinder, in which the azimuthal velocity plays an important role. The flow geometry is similar to the natural

convection flow, but the aspect ratio is 1. The flow is driven by co-/counter-rotating walls with constant angular speed Ω_t and Ω at top and bottom wall, and the cylinder is heated from top and cooled from bottom respectively with constant temperatures T_h and T_L ($T_h > T_L$), and the lateral wall is kept insulated.

A 200 × 100 lattice is employed in our simulation, the initial and boundary conditions are the same as Ref. [27], and the nondimensional parameters, which characterize the swirling flow, are set as follows: Pr = 1.0, Re = 1000 ($\mathrm{Re} = \Omega R^2/\nu$), Ri = 0, 1 ($\mathrm{Ri} = g\beta\triangle T/R\Omega^2$) and $s = -1$, 1 ($s = \Omega_t/\Omega$). The azimuthal velocity and isothermal lines predicted by present model are plotted in Figs. 7–10. As shown in Figs. 7 and 8, when Ri = 0 and $s = 1$, the top and bottom walls are rotating in the same direction with the same angular velocity, the azimuthal velocity and the isotherms are symmetric with respect to mid-height plane at $x = 1$, while the azimuthal velocity and the isotherms are antisymmetric at Ri = 0 and $s = -1$. Similar phenomena are also observed in Figs. 9 and 10 for Ri = 1 and $s = -1$, 1. It is also observed that the swirling motion is more confined in the vicinity of the top and bottom rotating walls, and the temperature profile is a linear distribution in the center of the domain as Ri increases to 1. These phenomena have been observed in Ref. [27]. For the quantitative comparison, the velocity components

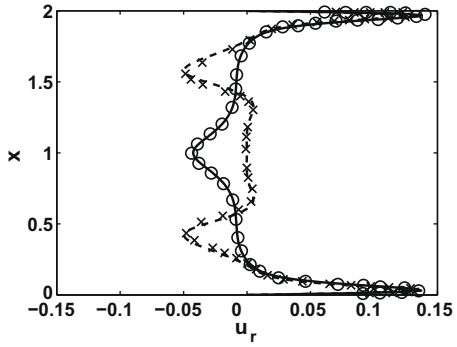

Fig. 11. Velocity profile of u_r along a vertical line at $r = 0.8$; Re = 1000. Symbols are from Ref. [27], lines are the LBE results. Open circle and solid line, Ri = 0, $s = -1$; cross and dashed line, Ri = 1.0, $s = -1$.

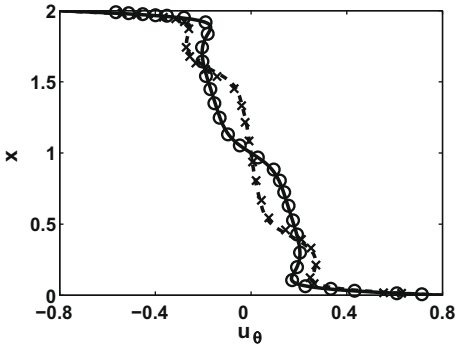

Fig. 12. Same as Fig. 11 but for u_θ.

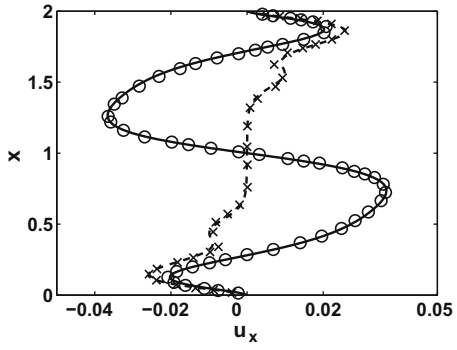

Fig. 13. Same as Fig. 11 but for u_x.

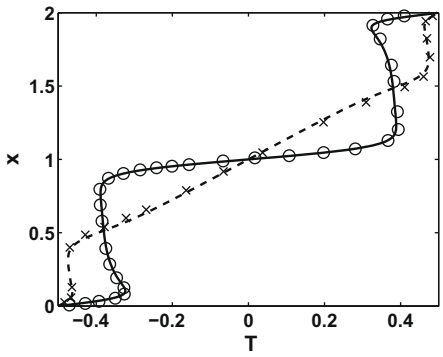

Fig. 14. Same as Fig. 11 but for temperature profile.

and the temperature profiles along the vertical line at $r = 0.8$ are compared with the numerical results of Ref. [27] in Figs. 11–14. It is found that the numerical results predicted by the present LBE agreed excellently with the previous work [27].

5. Conclusion

Axisymmetric thermal flows are frequently encountered in both science and engineering. Although the LBE method has achieved great success in simulating athermal/isothermal axisymmetric fluid flows, its applications for thermal axisymmetric flows are still not satisfactory. In this paper, we have proposed a thermal axisymmetric LBE model from the continuous Boltzmann equation. In this model, the temperature field can be simulated by a D2Q9 LBE model, and the model exhibits some distinct features that distinguish it from other previous LBE models [17–19]. First, the present thermal LBE model is derived from the kinetic theory, which has a solid foundation and clear physical significance; Second, the viscous dissipation term and work of pressure are naturally included by the present model, which are usually ignored in previous LBE models; Finally, unlike these thermal LBE models, there are no velocity and temperature gradients in the force terms by the present model.

Some numerical simulations including the thermal flow in a pipe, thermal buoyancy-driven flows, and swirling flows have been carried out to validate the proposed LBE model. It is found that the results predicted by the present model are in excellent agreement with analytical solutions and/or other numerical results.

Acknowledgments

This work is supported by the Program for NCET in University (NCET-07-0323) and the National Natural Science Foundation of China (50721005 and 60773195).

Appendix A. Derivation of the energy equation

Through the Chapman–Enskog expansion technique, we can introduce the following expansions:

$$\tilde{f} = \sum_{n=0}^{\infty} \epsilon^{(n)} \tilde{f}^{(n)}, \quad \partial_t = \sum_{n=0}^{\infty} \epsilon^{(n)} \partial_{t_n}, \quad \tilde{\phi} = \sum_{n=0}^{\infty} \epsilon^{(n)} \tilde{\phi}^{(n)}$$
$$\bar{f} = \sum_{n=0}^{\infty} \epsilon^{(n)} \bar{f}^{(n)}, \quad \bar{\phi} = \sum_{n=0}^{\infty} \epsilon^{(n)} \bar{\phi}^{(n)}, \quad \hat{f} = \sum_{n=0}^{\infty} \epsilon^{(n)} \hat{f}^{(n)}, \quad \widehat{\boldsymbol{\Phi}} = \sum_{n=0}^{\infty} \epsilon^{(n)} \widehat{\boldsymbol{\Phi}}^{(n)}.$$

With above expansions, Eqs. (5)–(7) can be written in consecutive orders of ϵ as

$$\epsilon^0 : \ \tilde{f}^{(0)} = \tilde{f}^{(eq)}, \quad \bar{f}^{(0)} = \bar{f}^{(eq)}, \quad \hat{f}^{(0)} = \hat{f}^{(eq)}, \tag{A1}$$

$$\begin{aligned} \epsilon^1 : \ & D_{t_0} \tilde{f}^{(0)} + \boldsymbol{a} \cdot \nabla_{\xi} \tilde{f}^{(0)} + \frac{\xi_r}{r} \tilde{f}^{(0)} + \frac{1}{r} \partial_{\xi_r} \hat{\phi}^{(0)} = -\frac{1}{\tau_f} \tilde{f}^{(1)}, \\ & D_{t_0} \bar{f}^{(0)} + \boldsymbol{a} \cdot \nabla_{\xi} \bar{f}^{(0)} + \frac{2\xi_r}{r} \bar{f}^{(0)} + \frac{1}{r} \partial_{\xi_r} \bar{\phi}^{(0)} = -\frac{1}{\tau_f} \bar{f}^{(1)}, \\ & D_{t_0} \hat{f}^{(0)} + \boldsymbol{a} \cdot \nabla_{\xi} \hat{f}^{(0)} - \boldsymbol{a} \cdot \boldsymbol{\xi} \tilde{f}^{(0)} - a_0 \bar{f}^{(0)} + \frac{\xi_r}{r} \hat{f}^{(0)} + \frac{1}{2r} \partial_{\xi_r} \widehat{\boldsymbol{\Phi}}^{(0)} = -\frac{1}{\tau_f} \hat{f}^{(1)}, \end{aligned} \tag{A2}$$

$$\begin{aligned}
\epsilon^2:\ & \partial_{t_1}\tilde{f}^{(0)} + D_{t_0}\tilde{f}^{(1)} + \boldsymbol{a}\cdot\nabla_{\xi}\tilde{f}^{(1)} + \frac{\xi_r}{r}\tilde{f}^{(1)} + \frac{1}{r}\partial_{\xi_r}\hat{\phi}^{(1)} = -\frac{1}{\tau_f}\tilde{f}^{(2)},\\
& \partial_{t_1}\bar{f}^{(0)} + D_{t_0}\bar{f}^{(1)} + \boldsymbol{a}\cdot\nabla_{\xi}\tilde{f}^{(1)} + \frac{2\xi_r}{r}\bar{f}^{(1)} + \frac{1}{r}\partial_{\xi_r}\bar{\phi}^{(1)} = -\frac{1}{\tau_f}\bar{f}^{(2)},\\
& \partial_{t_1}\hat{f}^{(0)} + D_{t_0}\hat{f}^{(1)} + \boldsymbol{a}\cdot\nabla_{\xi}\tilde{f}^{(1)} - \boldsymbol{a}\cdot\boldsymbol{\xi}\tilde{f}^{(1)} - a_\theta\bar{f}^{(1)} + \frac{\xi_r}{r}\hat{f}^{(1)} + \frac{1}{2r}\partial_{\xi_r}\widehat{\boldsymbol{\Phi}}^{(1)} = -\frac{1}{\tau_f}\hat{f}^{(2)},
\end{aligned} \tag{A3}$$

where $D_{t_0} = \partial_{t_0} + \boldsymbol{\xi}\cdot\nabla$, and we found that $\widehat{\boldsymbol{\Phi}}^{(n)}$ has similar properties to $\tilde{\phi}^{(n)}$ and $\bar{\phi}^{(n)}$ [16], which is given as

$$\int \partial_{\xi_r}\widehat{\boldsymbol{\Phi}}^{(n)}\,d\boldsymbol{\xi} = 0,\ \int \xi_\alpha\partial_{\xi_r}\widehat{\boldsymbol{\Phi}}^{(n)}\,d\boldsymbol{\xi} = -\delta_{r\alpha}\int \widehat{\boldsymbol{\Phi}}^{(n)}\,d\boldsymbol{\xi}. \tag{A4}$$

With these properties, the axisymmetric macroscopic equations at t_0 scale can be derived from Eq. (A2)

$$\partial_{t_0}\rho + \partial_\alpha(\rho u_\alpha) + \frac{\rho u_r}{r} = 0, \tag{A5}$$

$$\partial_{t_0}(\rho u_\alpha) + \partial_\beta(\rho u_\alpha u_\beta + p\delta_{\alpha\beta}) = \frac{\rho u_\theta^2}{r}\delta_{\alpha r} - \frac{\rho u_\alpha u_r}{r} + \rho a_\alpha, \tag{A6}$$

$$\partial_{t_0}(\rho u_\theta) + \partial_\beta(\rho u_\beta u_\theta) = -\frac{2\rho u_\theta u_r}{r} + \rho a_\theta, \tag{A7}$$

$$\partial_{t_0}\rho E + \partial_\alpha[(\rho E + p)u_\alpha] + \frac{(\rho E + p)u_r}{r} = \rho u_{0\alpha}a_\alpha. \tag{A8}$$

Similarly, from Eq. (A3), the macroscopic equations at t_1 scale can be obtained as follows:

$$\partial_{t_1}\rho = 0, \tag{A9}$$

$$\partial_{t_1}(\rho u_\alpha) + \partial_\beta P^{(1)}_{\alpha\beta} + \frac{1}{r}P^{(1)}_{\alpha r} - \frac{\delta_{\alpha r}}{r}\int \tilde{\phi}^{(1)}\,d\boldsymbol{\xi} = 0, \tag{A10}$$

$$\partial_{t_1}(\rho u_\theta) + \partial_\beta Q^{(1)}_\beta + \frac{2}{r}Q^{(1)}_r = 0, \tag{A11}$$

$$\partial_{t_1}(\rho E) + \partial_\beta T^{(1)}_\beta + \frac{1}{r}T^{(1)}_r = 0, \tag{A12}$$

where $P^{(1)}_{\alpha\beta} = \int \xi_\alpha\xi_\beta\tilde{f}^{(1)}\,d\boldsymbol{\xi},\ Q^{(1)}_\beta = \int \xi_\beta\bar{f}^{(1)}\,d\boldsymbol{\xi},\ T^{(1)}_\beta = \int \xi_\beta\hat{f}^{(1)}\,d\boldsymbol{\xi}$.

In order to recover the macroscopic equations, the terms of $P^{(1)}_{\alpha\beta},\ Q^{(1)}_\beta$ and $T^{(1)}_\beta$ in the t_1 scale equations must be estimated. From Eqs. (A2), (A5)–(A8), these terms can be evaluated as

$$-\frac{1}{\tau_f}P^{(1)}_{\alpha\beta} = p\left[(\partial_\alpha u_\beta + \partial_\beta u_\alpha) - \left(\partial_\gamma u_\gamma + \frac{u_r}{r}\right)\delta_{\alpha\beta}\right], \tag{A13}$$

$$-\frac{1}{\tau_f}Q^{(1)}_\alpha = -\frac{pu_\theta}{r}\delta_{\beta r} + p\partial_\beta u_\theta, \tag{A14}$$

$$-\frac{1}{\tau_f}T^{(1)}_\alpha = c_p p\partial_\alpha T + pu_\beta\left[\partial_\alpha u_\beta + \partial_\beta u_\alpha - \left(\partial_\gamma u_\gamma + \frac{u_r}{r}\right)\delta_{\alpha\beta}\right] + pu_\theta\partial_\alpha u_\theta - \frac{pu_\theta^2}{r}\delta_{\alpha r}. \tag{A15}$$

With the above results and coupled the t_0, t_1 time scales, the macroscopic axisymmetric equations can be recovered as

$$\partial_t\rho + \partial_\alpha(\rho u_\alpha) + \frac{\rho u_r}{r} = 0, \tag{A16}$$

$$\begin{aligned}
\partial_t(\rho u_\alpha) + \partial_\beta(\rho u_\alpha u_\beta + p\delta_{\alpha\beta}) = {} & \partial_\beta\left[\mu\left(\partial_\alpha u_\beta + \partial_\beta u_\alpha - \left(\partial_\gamma u_\gamma + \frac{u_r}{r}\right)\delta_{\alpha\beta}\right)\right] + \frac{\mu}{r}\left[\partial_\alpha u_r + \partial_r u_\alpha - \left(\partial_\gamma u_\gamma + \frac{u_r}{r}\right)\delta_{\alpha r}\right]\\
& + \frac{\rho u_\theta^2}{r}\delta_{\alpha r} - \frac{\rho u_\alpha u_r}{r} - \frac{2\mu}{r^2}u_r\delta_{\alpha r} + \rho a_\alpha,
\end{aligned} \tag{A17}$$

$$\partial_t(\rho u_\theta) + \partial_\beta(\rho u_\beta u_\theta) = \partial_\beta(\mu\partial_\beta u_\theta) - \frac{2\rho u_\theta u_r}{r} - \frac{\mu}{r}\left(u_\theta\partial_r\ln\rho - \partial_r u_\theta + \frac{u_\theta}{r}\right) + \rho a_\theta, \tag{A18}$$

$$\begin{aligned}
\partial_t\rho E + \partial_\alpha[(\rho E + p)u_\alpha] + \frac{1}{r}[(\rho E + p)u_r] = {} & \partial_\alpha(\lambda\partial_\alpha T) + \partial_\alpha\left[\mu u_\beta\left(\partial_\alpha u_\beta + \partial_\beta u_\alpha - \left(\partial_\gamma u_\gamma + \frac{u_r}{r}\right)\delta_{\alpha\beta}\right)\right] + \partial_\alpha(\mu u_\theta\partial_\alpha u_\theta)\\
& - \partial_r\left(\frac{\mu u_\theta^2}{r}\right) + \frac{1}{r}\left[\lambda\partial_r T + \mu\left(u_\beta\left(\partial_r u_\beta + \partial_\beta u_r - \left(\partial_\gamma u_\gamma + \frac{u_r}{r}\right)\delta_{r\beta}\right)\right)\right.\\
& \left. + \mu u_\theta\partial_r u_\theta - \frac{\mu u_\theta^2}{r}\right] + \rho u_{0\alpha}a_\alpha,
\end{aligned} \tag{A19}$$

where $\mu = \tau_f p$ is the dynamic viscosity and $\lambda = c_p \tau_f p$ is the thermal conductivity which limited to fixed Prandtl number. This problem can be removed by introducing a modified collision operator in Eq. (7).

References

[1] S.F. Lang, A. Vidal, A. Acrivos, Buoyancy-driven convection in cylindrical geometries, J. Fluid. Mech. 36 (1969) 239–256.
[2] D.R. Otis, J. Roessler, Development of stratification in a cylindrical enclosure, Int. J. Heat Mass Transfer 30 (1987) 1633–1636.
[3] A. Lemembre, J.P. Petit, Laminar natural convection in a laterally heated and upper cooled vertical cylindrical enclosure, Int. J. Heat Mass Transfer 41 (1998) 2437–2454.
[4] R. Benzi, S. Succi, M. Vergassola, The lattice Boltzmann equation: theory and applications, Phys. Rep. 222 (1992) 145–197.
[5] S. Succi, The Lattice Boltzmann Equation for Fluid Dynamics and Beyond, Oxford University Press, Oxford, 2001.
[6] S. Chen, G. Doolen, Lattice Boltzmann method for fluid flows, Annu. Rev. Fluid Mech. 30 (1998) 329–364.
[7] X.D. Niu, C. Shu, Y.T. Chew, An axisymmetric lattice Boltzmann model for simulation of Taylor–Couette flows between two concentric cylinders, Int. J. Mod. Phys. C 14 (2003) 785–796.
[8] M.E. McCracken, J. Abraham, Simulations of liquid break up with an axisymmetric, multiple relaxation time, index-function lattice Boltzmann model, Int. J. Mod. Phys. C 16 (2005) 1671–1692.
[9] T.S. Lee, H. Huang, C. Shu, An axisymmetric incompressible lattice BGK model for simulation of the pulsatile flow in a circular pipe, Int. J. Numer. Methods Fluids 49 (2005) 99–116.
[10] I. Halliday, L.A. Hammond, C.M. Care, et al, Lattice Boltzmann equation hydrodynamics, Phys. Rev. E 64 (2001) 011208.
[11] T.S. Lee, H. Huang, C. Shu, An axisymmetric incompressible lattice Boltzmann model for pipe flow, Int. J. Mod. Phys. C 17 (2006) 645–661.
[12] T. Reis, T.N. Phillips, Modified lattice Boltzmann model for axisymmetric flows, Phys. Rev. E 75 (2007) 056703.
[13] T. Reis, T.N. Phillips, Numerical validation of a consistent axisymmetric lattice Boltzmann model, Phys. Rev. E 77 (2008) 026703.
[14] J.G. Zhou, Axisymmetric lattice Boltzmann method, Phys. Rev. E 78 (2008) 036701.
[15] S. Chen, J. Tölke, S. Geller, M. Krafczyk, Lattice Boltzmann model for incompressible axisymmetric flows, Phys. Rev. E 78 (2008) 046703.
[16] Z.L. Guo, H.F. Han, B.C. Shi, C.G. Zheng, Theory of the lattice Boltzmann equation: lattice Boltzmann model for axisymmetric flows, Phys. Rev. E 79 (2009) 046708.
[17] Y. Peng, C. Shu, Y.T. Chew, J. Qiu, Numerical investigation of flows in Czochralski crystal growth by an axisymmetric lattice Boltzmann method, J. Comput. Phys. 186 (2003) 295–307.
[18] H. Huang, T.S. Lee, C. Shu, Hybrid lattice Boltzmann finite-difference simulation of axisymmetric swirling and rotating flows, Int. J. Numer. Methods Fluids 53 (2007) 1707–1726.
[19] S. Chen, J. Tölke, M. Krafczyk, Simulation of buoyancy-driven flows in a vertical cylinder using a simple lattice Boltzmann model, Phys. Rev. E 79 (2009) 016704.
[20] L. Zheng, B.C. Shi, Z.L. Guo, C.G. Zheng, Lattice Boltzmann equation for axisymmetric thermal flow, Comput. Fluids 39 (2010) 945–952.
[21] Z.L. Guo, C.G. Zheng, B.C. Shi, T.S. Zhao, Thermal lattice Boltzmann equation for low Mach number flows: decoupling model, Phys. Rev. E 75 (2007) 036704.
[22] R.S. Maier, R.S. Bernard, D.W. Grunau, Boundary conditions for the lattice Boltzmann method, Phys. Fluids 8 (1996) 1788–1801.
[23] A.M. Artoli, A.G. Hoekstra, P.M.A. Sloot, 3D pulsatile flow with the lattice Boltzmann BGK method, Int. J. Mod. Phys. C 13 (2002) 1119–1134.
[24] S.K. Bhaumik, K.N. Lakshmisha, Lattice Boltzmann simulation of lid-driven swirling flow in confined cylindrical cavity, Comput. Fluids 36 (2007) 1163–1173.
[25] S. Chapman, T.G. Cowling, The Mathematical Theory of Non-Uniform Gases, third ed., Cambridge University Press, Cambridge, 1970.
[26] Z.L. Guo, C.G. Zheng, B.C. Shi, An extrapolation method for boundary conditions in lattice Boltzmann method, Phys. Fluids 14 (2002) 2007–2010.
[27] R. Iwatsu, Numerical study of swirling flows in a cylindrical container with co-/counter-rotating end disks under stable temperature difference, Int. J. Heat Mass Transfer 48 (2005) 4854–4866.